Materials Today Sustainability 30 (2025) 101124

Contents lists available at ScienceDirect

Materials Today Sustainability

journal homepage: www.journals.elsevier.com/materials-today-sustainability

Insights into the stability of copper gas diffusion electrodes for carbon dioxide reduction at high reaction rates

Nicolò B.D. Monti [a,b], Gumaa A. El-Nagar [c], Marco Fontana [a,b], Felicia Di Costola [a,b], Siddharth Gupta [c], Matthew T. Mayer [c,**], Candido F. Pirri [a,b], Juqin Zeng [a,b,*]

[a] Istituto Italiano di Tecnologia - IIT, Centre for Sustainable Future Technologies (CSFT), Via Livorno 60, Turin, 10144, Italy
[b] Department of Applied Science and Technology (DISAT), Politecnico di Torino, Corso Duca degli Abruzzi 24, Turin, 10129, Italy
[c] Helmholtz Young Investigator Group: Electrochemical Conversion, Helmholtz-Zentrum Berlin für Materialien und Energie, Hahn-Meitner-Platz 1, 14109, Berlin, Germany

ARTICLE INFO

Keywords:
Carbon dioxide
Electrocatalysis
Ethylene
Copper
Operando X-ray absorption spectroscopy

ABSTRACT

Electrosynthesis of value-added chemicals from CO_2 offers a sustainable solution to climate change, renewable energy use, and raw material shortages. This study examines the high-rate production of ethylene (C_2H_4) and ethanol (CH_3CH_2OH) through CO_2 reduction reaction on copper (Cu) gas diffusion electrodes (GDEs) made by sputtering deposition. The catalyst layer thickness of the GDEs, adjusted by deposition time, significantly affects the electrode stability. During testing, a selectivity shift is observed, where C_2H_4 and CH_3CH_2OH selectivity decreases, while CH_4 and H_2 selectivity increases. However, an alternating operation by interrupting and restarting the polarization fully restores the C_2H_4 and CH_3CH_2OH selectivity. *Operando* X-ray absorption spectroscopy with online product analysis reveals that at constant potentials, the dominant oxidized Cu species gradually reduces to metallic Cu, along with a decline in C_2H_4 selectivity. Under alternating operation, some oxidized Cu species remains, and the C_2H_4 selectivity is also preserved. This outcome suggests a close link between cationic Cu species and C_2H_4 production, offering insights into stabilizing these species for prolonged C_2H_4 production.

1. Introduction

Among many emerging technologies aiming at a sustainable future, the electrochemical conversion of carbon dioxide (CO_2) into value-added chemicals and fuels has been becoming utmost appealing, since it can increase the utilization efficiency of intermittent renewable electricity by storing it in chemical form, while transforming CO_2 waste into valuable feedstocks. The produced chemicals and fuels are highly applicable to the transportation and energy sectors as well as chemical industries, alleviating the dependence of our society on fossil fuels. However, the electrochemical CO_2 reduction reaction (CO_2RR) is energetically and atomically inefficient, since it requires high energy input to overcome the large kinetic overpotentials and shows many difficulties in controlling the selectivity toward desired products [1,2]. The particularly negative potentials required for the CO_2RR cause the instability of cathode materials. Hence, this reaction calls for catalysts with good activity, selectivity, and stability to achieve satisfactory operability for practical application. During the last decade, intensive research has focused on the development of catalysts for the CO_2RR to different targeted products such as carbon monoxide (CO) [3–6], formic acid (HCOOH) [7–12], methane (CH_4) [13,14], ethylene (C_2H_4) [15–17] and ethanol (C_2H_5OH) [18–20]. Among them, C_2H_4 and C_2H_5OH are considered the most attractive targets, due to their high market volumes as well as decent market prices [21]. For catalyzing the CO_2RR to C_2H_4, copper (Cu)-based materials show unique capability, as suggested by the early experimental studies by Hori et al. [22], as well as the computational investigations by Nørskov et al. [23,24]. Recent studies maintained that Cu-based catalysts are the best candidates for this purpose, and Cu thin layer catalyst [25], CuO_x derived Cu [17], halogen-modified Cu [26], polyamine-modified Cu [16], and bimetallic CuAl [27,28] resulted in the state-of-the-art performance. Despite the encouraging progress, the industrial implementation of this technology is still

* Corresponding author. Istituto Italiano di Tecnologia - IIT, Centre for Sustainable Future Technologies (CSFT), Via Livorno 60, Turin, 10144, Italy.
** Corresponding author. Helmholtz Young Investigator Group: Electrochemical Conversion, Helmholtz-Zentrum Berlin für Materialien und Energie, Hahn-Meitner-Platz 1, 14109, Berlin, Germany.
E-mail addresses: m.mayer@helmholtz-berlin.de (M.T. Mayer), juqin.zeng@polito.it (J. Zeng).

https://doi.org/10.1016/j.mtsust.2025.101124
Received 15 January 2025; Received in revised form 3 April 2025; Accepted 19 April 2025
Available online 19 April 2025

considerably hindered by the limited stability of C_2H_4 production on Cu-based electrodes, which could be related to the restructuring of catalysts [29–31], the deposition of carbonate salts in the GDE [32], the degradation of electrode/electrolyte interface [33] and so on. Many methods have been employed to mitigate such problems, including the development of more advanced catalysts [34], the utilization of highly hydrophobic substrates [35], and the design of new cell configurations [36]. However, significant work is still needed to fully understand the stability challenges and extend the operational lifespan to meet industry requirements.

In this work, we comprehensively studied the effects of the electrode thickness, the test protocols and the electrolyte concentrations on the stability characteristics of Cu-based GDEs fabricated with a fast and scalable sputtering deposition route. Compared to ink-based methods for GDEs preparation with powder-like catalysts, the sputtering deposition ensures more precise control of the thickness, easier tailoring of the composition, better adhesion to the substrate that leads to higher electrical conductivity, and much less time and labor [37]. The CO_2RR experiments show that both catalyst layer thickness and surface chemical composition of the Cu GDEs, as well as the test protocol and employed electrolyte, significantly influence the stability for C_2H_4 and C_2H_5OH production.

2. Experimental section

2.1. Preparation of Cu electrodes

A magnetron sputter coater (Quorum Technologies Ltd Q150T) was used to prepare the GDEs. Copper disc (99.99 %, Testbourne) was used as target to deposit Cu directly on a Gas Diffusion Layer (GDL). This last was a carbon paper (GDL; SIGRACET 28BC, Ion Power GmbH) used as the substrate, in which a microporous layer and a certain amount of polytetrafluoroethylene were incorporated to enhance gas diffusion, and hence to ensure the performances of GDEs[3,38–40]. The preparation of Cu GDEs was carried out at 50 mA with deposition durations ranging from 50 to 1200 s. The samples are denoted as Cu_X, where X indicates the deposition time in seconds and equals to 50, 100, 200, 300, 400, 600, 800, 1000 and 1200.

2.2. Physical and chemical characterization

The morphological investigation of the Cu electrodes by Field Emission Scanning Electron Microscopy (FESEM) and the localized preparation of cross-sections with Focused Ion Beam (FIB) were performed with a dual-beam FIB-FESEM workstation (Auriga by Zeiss). Energy Dispersive X-ray (EDX) Spectroscopy spectra were acquired with a X-max Silicon Drift Detector (50 mm^2 active area) by Oxford Instruments. Concerning the preparation of the cross-sections, Ga^+ ions were accelerated with 30 kV voltage and different ion currents were used for milling (2 nA) and cleaning (600 pA). In order to preserve the surface of the Cu electrodes, a protective Pt layer was deposited by ion-beam induced deposition inside the FIB-SEM chamber.

2.3. Electrochemical tests and product analyses

The CO_2RR experiments were conducted in a commercial three-compartment three-electrode flow cell (Electrocell A/S), as illustrated in Fig. S1 and described in the supporting information (SI). Both potentiostatic and galvanostatic modes were used to perform the CO_2 electrolysis. The reported potentials were rescaled to the reversible hydrogen electrode (RHE) using the Nernst equation. Unless otherwise specified, all potentials are referenced to the RHE, as shown in Equation (1),

$$E_{RHE} = E_{Appl.} + E_{Ag/AgCl(3M\ Cl^-)} + 0.0591 * pH \quad \text{Equation 1}$$

where E_{RHE} is the potential referring to the RHE; $E_{Appl.}$ is the measured potential during the galvanostatic or applied potential in chronoamperometric tests; $E_{Ag/AgCl(3M\ Cl^-)}$ is the potential of the reference electrode and pH is the bulk *pH* value of the electrolyte. The bulk *pH* was monitored during the electrolysis and maintained almost a constant value.

Gas-phase products were analyzed on-line by a micro gas chromatograph (μGC, Fusion®, INFICON), which was composed of two channels with a 10 m Rt-Molsieve 5A column and an 8 m Rt-Q-Bond column, respectively, and each channel with a micro thermal conductivity detector. The faradaic efficiency (FE) for each gas-phase product was determined from its concentration in the outlet gas stream, as shown in Equation (2),

$$FE = \frac{V * t * C * n * F}{V_m * Q} \quad \text{Equation 2}$$

where V_m is the molar volume of an ideal gas (L mol^{-1}); V is the flow rate of gas measured at the outlet of the cathodic side collecting the gas from both CO_2 compartment and catholyte compartment (L min^{-1}); t is electrolysis time (min); Q is the total charge passed through the system during the electrolysis time t (coulombs, C); C is the concentration of the gas product (% v/v); n is the number of electrons required to obtain 1 molecule of this product ($n = 2$ for CO and H_2, $n = 8$ for CH_4 and $n = 12$ for C_2H_4 formation); F is the Faraday constant (96485 C mol^{-1}).

Quantification of liquid products was estimated by collecting aliquots directly from the catholyte at the output at different time intervals during the measurements and analyzing them using a high-performance liquid chromatograph (Nexera Series, Shimadzu HPLC). The HPLC was equipped with a Photo Diode Array detector and a Refractive Index Detector, and a ReproGel H+ (Dr Maisch 300 × 8 mm) column. A solution of 9.0 mM H_2SO_4 (flow rate of 1.0 mL min^{-1}) was used as the mobile phase. The FE of the liquid products was calculated from its concentration in the solution using Equation (3),

$$FE = \frac{v * C * n * F}{Q} \quad \text{Equation 3}$$

where v is the volume of catholyte (L); C is the concentration of the liquid product (mol L^{-1}); n is the number of electrons required to obtain 1 molecule of this product ($n = 2$ for $HCOO^-$, $n = 8$ for CH_3COO^-, $n = 12$ for CH_3CH_2OH formation); F is the Faraday constant (96485 C mol^{-1}); Q is the total charge passed through the system during the test (coulombs, C).

2.4. Operando X-ray absorption spectroscopy (XAS)

The Cu K-edge XAS measurements were conducted at the KMC-2 beamline at BESSY II in Berlin [41]. Spectra were collected in fluorescence mode using an energy-dispersive detector. XAS was performed in an adapted catholyte-flow electrochemical reactor equipped with an X-ray transparent window (Kapton tape), maintaining the gas flow pattern and overall cell geometry to ensure the reproducibility of laboratory results during *operando* XAS measurements (see Fig. S2). X-ray absorption near edge structure (XANES) and extended X-ray absorption fine structure (EXAFS) spectra were recorded in the energy range of 8779–9729 eV (K = 14) for cells operating at a constant current of 200 mA cm^{-2}, either operated continuously (non-pulsing) or interrupted every hour for 1 min at open circuit (pulsing). Each EXAFS spectrum required approximately 17 min, and at least three consecutive repetitions per experiment were collected and averaged. Cu K-edge reference spectra for metallic Cu, Cu_2O, $Cu(OH)_2$, basic Cu carbonate ($Cu_2(OH)_2CO_3$), and CuO were obtained in transmission mode using pellets made from their respective diluted powders with cellulose [42]. All XAS data were processed using Athena software from the Demeter software suite, with the metallic Cu spectrum serving as reference for

energy calibration [42].

3. Results and discussion

3.1. Physical and chemical characterization

The Cu loadings of all Cu_X electrodes were evaluated by weighing the GDL substrate before and after the Cu deposition. As shown in Fig. 1, the Cu loading increases linearly with raising the sputtering time, indicating a reliable deposition process. The Cu deposition rate was extrapolated from the slope of the plot correlating Cu loading and deposition time, and it is estimated to be 0.34 μg cm^{-2} s^{-1}.

To evaluate the thickness of the Cu layers, cross-sections of the selected samples were analyzed using FESEM-FIB measurements. Fig. 2a shows the cross-section of Cu_{800} electrode. The Pt film was deposited on top of the GDE using FIB to precisely measure the thickness of the Cu layer, which was estimated to be approximately 560 nm. Similar analysis was performed on Cu_{300} and Cu_{1200} electrodes, with the results summarized in Fig. 2b. It is clear that the thickness of the deposited Cu layer increases proportionally with the deposition time, mirroring the trend in Cu mass loading. The top view of Cu_{800} electrode shows the porous nature of the Cu layer with sub-micrometric nanoparticles aggregation (Fig. 2c and d). A similar morphology was observed for all electrodes (see Supporting Information for additional FESEM characterization).

3.2. Effects of Cu layer thickness on CO_2RR performance

The electrochemical performance of the GDEs with different Cu loadings was firstly evaluated at −1.2 V_{RHE} in potentiostatic mode. The FE and partial current density for each product are summarized in Fig. 3a and b, respectively. All electrodes show overall FE of gaseous products close to 70–80 % with C_2H_4 and CO as dominant products. The selectivity of C_2H_4 increases with the sputtering time (thickness and loading of Cu layer), reaching a plateau at a sputtering time of 400 s or higher, while the CO selectivity exhibits the opposite trend. The thinnest electrode, Cu_{50}, displays a selectivity of 33 % for C_2H_4, which is enhanced to 45 % for thicker electrodes (sputtering time ≥400 s). Instead, the FE_{CO} is 37 % for Cu_{50}, dropping to 22 % for Cu_{400}, and further decreasing to 15 % for thicker electrodes (sputtering time ≥800 s). This behavior could be attributed to the prolonged retention time of CO, the key intermediate for C_2H_4, as the thickness of the catalyst layer increases. This extended time facilitates the dimerization of CO into C_2H_4 [31,43]. CH_4 and H_2 are minor products, and count for less than 15 % for all electrodes. These results are consistent with the literature

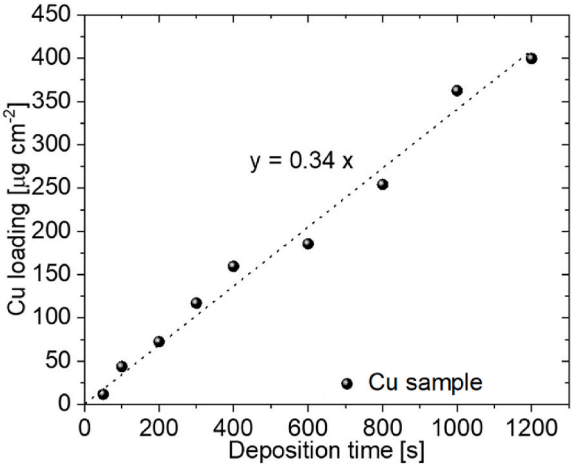

Fig. 1. Cu mass loading as a function of deposition time. The dash line is resulted from the linear fitting of the experimental data (black spheres).

[15,19,44,45]. Ren et al.'s study [15] investigated several thicknesses of Cu_2O in a batch cell, and obtained similar product distribution but with higher FE_{H2} compared to herein presented results. In our study, the use of a flow cell and 1 M KOH electrolyte increases the selectivity towards C_2H_4 thanks to the suppression of HER and CH_4 due to the highly alkaline electrolyte [1]. The detected liquid products include $HCOO^-$, CH_3COO^- and CH_3CH_2OH. Interestingly, the selectivity of the first two compounds remains similar on thin and thick samples, while the last one shows significantly higher FEs on thick samples. The selectivity trend for CH_3CH_2OH mirrors that of C_2H_4, attributing to a strong correlation of their formation pathways [18]. The $FE_{CH3CH2OH}$ increases with the thickness of Cu layer, reaching a plateau of 20 % on thick Cu_x electrodes (x > 400 s).

The Cu_{50} electrode shows a geometric current density of 140 mA cm^{-2}, which rises almost constantly to 247 mA cm^{-2} for Cu_{1200}, as shown in Fig. S3. The increase of current as well as CH_3CH_2OH and C_2H_4 selectivity with prolonging the sputtering time leads to an almost constant increase of partial current density for C_2 products, which peaks at 170 mA cm^{-2}, as reported in Fig. 3b. All other products with the exception of CO have a higher formation rate when increasing the catalyst thickness, indicated by the increasing partial current densities. The difference in the CO production on thin and thick electrodes is likely related to the prolonged retention time of CO in the latter that favours its dimerization [31,43], as previously discussed. To understand the intrinsic activity of various electrodes, the electrochemical active surface area (ECSA) was evaluated, as detailed in SI.Figure S4 reports the evaluated double layer capacitance, which increases proportionally with the catalyst loading. By dividing this value by the specific capacitance of a flat Cu electrode (40 μF cm^{-2}) [46,47], we obtained the ECSA values. When dividing the geometric current density reported in Fig. S3 by ECSA, we obtained an almost constant specific current density of 0.38 mA cm^{-2}_{ECSA} for all electrodes. This outcome indicates comparable intrinsic activity of Cu_x electrodes, probably attributed to their similar physical and chemical properties.

Each test lasted for several hours to evaluate the electrode stability and study the product distribution along test time (Fig. S5). Increasing Cu thickness can enhance the stability of the electrodes. Cu_{600} and Cu_{800} have a stable selectivity for C_2H_4 that remains higher than 40 % for more than 1 h, and this stability is further enhanced on Cu_{1000} and Cu_{1200} electrodes. At the end of the tests, the electrodes are likely to be flooded or choked since H_2 becomes the main product.

The enhancement of the stability on thicker samples could be attributed to different factors. Firstly, larger thickness results in a bigger loading of catalyst and high surface area, indicating a longer time for restructuring under working conditions [29,48,49]. The restructuring could include the catalyst oxidation state, morphology, grain boundaries, defective sites [30,50], which can affect the CO_2RR products distribution on Cu. Secondly, it could take more time for cations and water to penetrate through a thicker catalyst layer, causing the electrode choking by salt deposition and flooding [2,51]. FESEM characterization of the samples after CO_2RR testing at the timescale of hour confirms the evolution of morphology of the catalysts, suggesting reconstruction of the surface under operating conditions (see Fig. S6). Concerning the thinner electrodes, they probably undergo dissolution into the electrolyte, as confirmed by the reduced Cu content detected by EDX spectroscopy (see Table S1). Cu dissolution and salt precipitation (confirmed by EDX, Table S1) may be the main mechanisms involved in the limited stability of the thinner samples at the considered timescales. The aforementioned phenomena are mitigated with increasing thickness of the Cu layer, as confirmed by FESEM (Fig. S6) and EDX (Table S1).

3.3. Effects of test process on CO_2RR performance

It is interesting to note a selectivity change for products (particularly CH_4 and C_2H_4) before sharp increase of H_2 (electrode failure), as shown in Fig. S5. In order to understand this phenomenon, further tests have

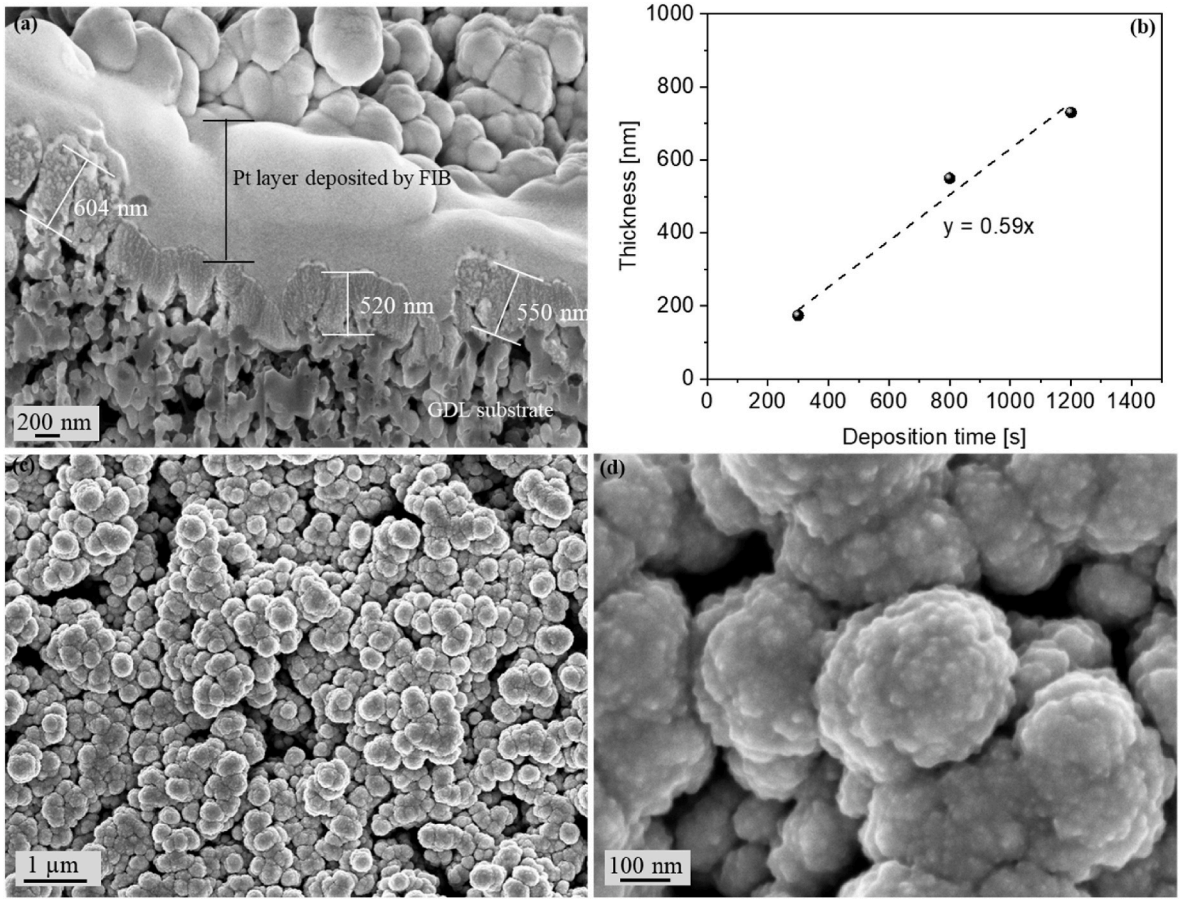

Fig. 2. FESEM images: (a) cross-section view of Cu_{800} electrode, (b) Cu thickness as a function of time (fitting R^2 is 0.998), (c) and (d) top view of Cu_{800} electrode.

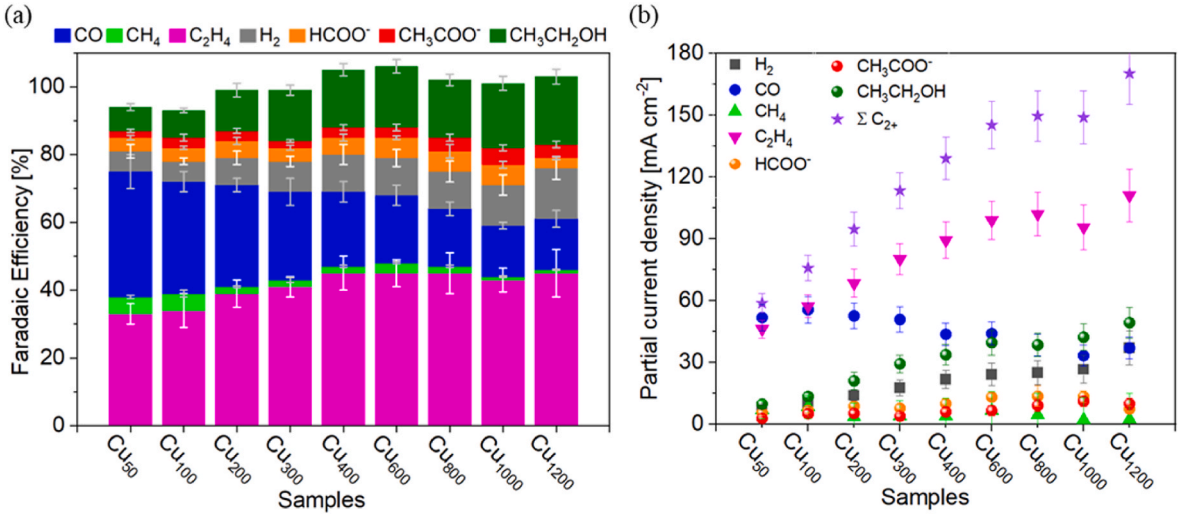

Fig. 3. CO_2RR tests on Cu GDEs at −1.2 V_{RHE}: (a) faradaic efficiency distribution and (b) partial current densities. The uncertainties were obtained from at least three independent replicate experiments.

been performed on Cu_{800} electrode with the flow cell in a galvanostatic mode. This electrode was chosen due to its good selectivity and stability with respect to other electrodes. Despite good performance of its counterparts Cu_{1000} and Cu_{1200}, we observed that some parts of these electrodes were peeled off after testing, probably due to their excess thickness. Since no binder was added into the Cu layer, the fast gas evolution during the reaction could lead to the detachment of the Cu powder from the thick electrodes.

Firstly, the performance of Cu_{800} electrode was investigated across a wide range of current density (150–900 mA cm^{-2}), as shown in Fig. 4a. Increasing current density until 450 mA cm^{-2} enhances the maximum FE_{C2H4} up to 46 % and a C_2H_4 partial current of 208.7 mA cm^{-2}. The latter further rises to 216 mA cm^{-2} at a geometric current density of 600 mA cm^{-2}. It is worth noting that the partial current density for

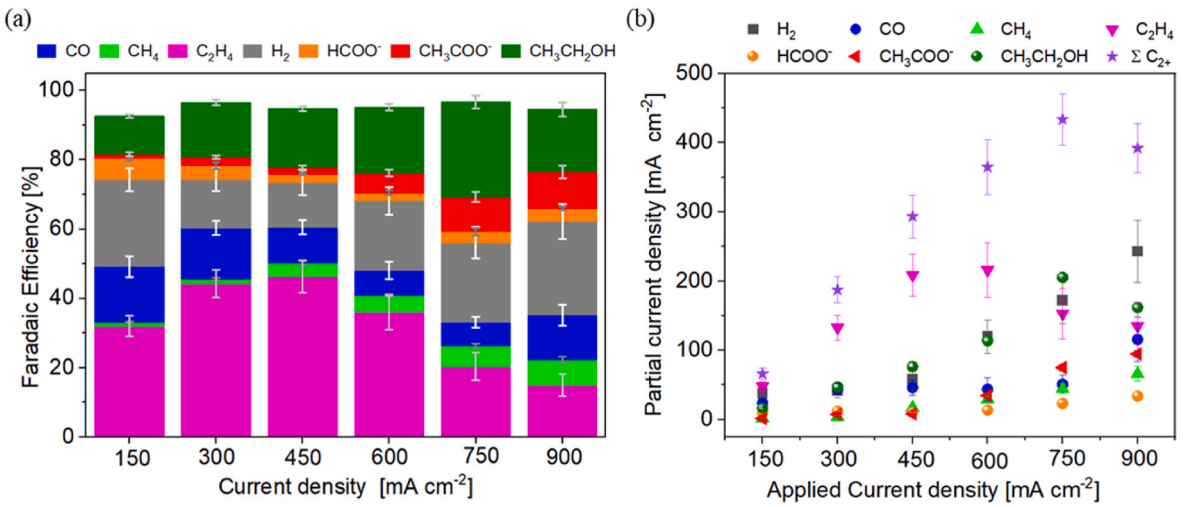

Fig. 4. CO_2 electrolysis on Cu_{800} electrode at various current densities: (a) Faradaic efficiency distribution and (b) Partial current density of each CO_2RR product. (The reported uncertainties were obtained from at least three independent replicate experiments.)

CH_3CH_2OH increases fast with raising the geometric current density until 750 mA cm^{-2}, reaching a maximum value of 205.4 mA cm^{-2}. A shift in selectivity from C_2H_4 to CH_3CH_2OH at high current densities has been reported in the literature [14,20], which is attributed to the destabilization of C_2H_4 formation, favoring CH_3CH_2OH pathway, at very high local pH induced by high reaction rates [20]. However, the selectivity of C_2H_4 and CH_3CH_2OH is closely correlated since their formation shares a common reaction intermediate *CH–COH [18]. The highest current density of 423 mA cm^{-2} is achieved for the formation of C_2 products at a geometric current density of 750 mA cm^{-2}, as reported in Fig. 4b. The partial current density dedicated to other products is almost stationary with applied current density.

The stability of Cu_{800} along test time was analyzed in detail at a geometric current density of 200 mA cm^{-2}. During the measurement, the product selectivity changes, as shown in Fig. 5. The Cu_{800} sample shows an initial FE_{H2} of 10 %, FE_{CO} of 12 %, FE_{CH4} of 1 %, FE_{C2H4} of 41 %, FE_{HCOO-} of 4 %, $FE_{CH3COO-}$ of 2 % and $FE_{CH3CH2OH}$ of 21 %. These results are in agreement with the similar reported work [52]. The CO selectivity rapidly decreases after 40 min. FE_{C2H4} and $FE_{CH3CH2OH}$ follow a similar trend and are stable for almost an hour close to 40 % and 20 %, respectively. Successively, the losses of FE_{C2H4} and $FE_{CH3CH2OH}$ are accompanied by the significant increase of FE_{CH4} and FE_{H2}, and slight rise in other liquid products. At the end of the test, all CO_2RR products have FE values lower the 10 %, while the H_2 becomes dominant. This phenomenon could be related to the electrode failure due to flooding and salt deposition[53–55]. The same observation was found on samples with different thicknesses, as shown in Fig. S5 with only gas product distribution. All electrodes show a similar selectivity switch trend, but at different test time before electrode failure. The correlation between the time for selectivity switch and the thickness or loading of the catalyst could be attributed to different factors such as the amount of oxide present in the catalyst layer and the salt and water accumulation across the catalyst layer. Under steady-state (constant current) operation, the catalyst material and its local environment can change over time, possibly contributing to the degradation of performance.

We hypothesize that periodically pausing cell operation by switching to an open circuit could stabilize or restore the electrode properties and local environment, potentially recovering the electrode performance. Hence, we conducted extended testing under 200 mA cm^{-2} in which the current was periodically interrupted and restarted. Whenever the FE_{C2H4} decreased to 20 %, the electrode was subjected to open circuit for 1 min, followed by resuming the operation at 200 mA cm^{-2}. As shown in Fig. 6, this process is effective in recovering the electrode behavior, including the selectivity and the potential. In each cycle, the FE_{C2H4} and $FE_{CH3CH2OH}$ are regained initially, followed by a gradual decrease along test time, while the initially restored FE_{CH4}, FE_{H2}, FE_{HCOO-} and $FE_{CH3COO-}$

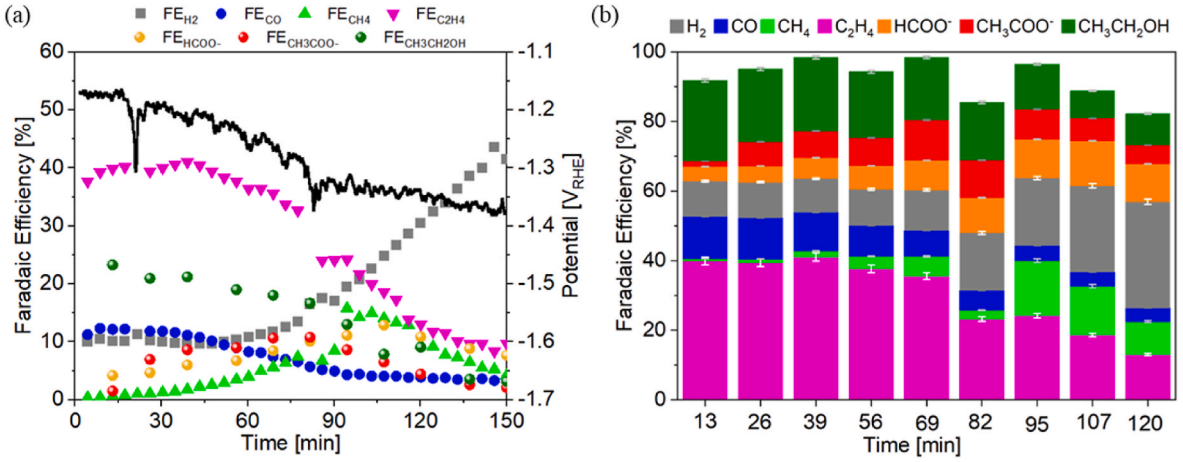

Fig. 5. CO_2RR on Cu_{800} electrode at 200 mA cm^{-2}: (a) product distribution as a function of time and (b) FE details at sampling time. The long-term measurements were independently conducted multiple times, yielding very similar results. One experiment has been chosen to represent the results. In this scenario, the uncertainty in the distribution of the FE distribution arises from the combination of instrument calibration error and instrumental parameters.

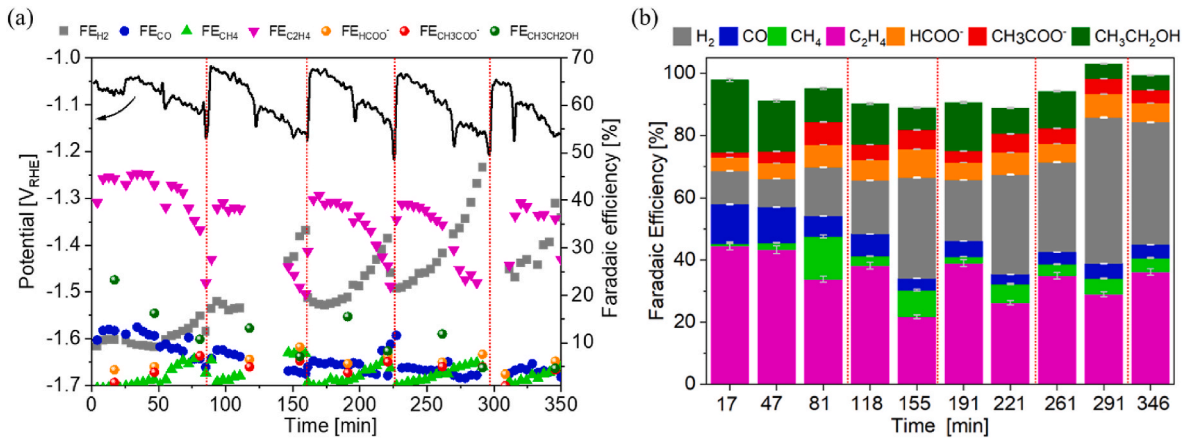

Fig. 6. CO_2RR on Cu_{800} electrode at pulsed current density 200 mA cm^{-2}: (a) FE distribution during the measurements (the vertical red dot lines indicating the moments where the cell operation was paused) and (b) all products FE at sampling time. The long-term measurements were independently conducted multiple times, yielding very similar results. One experiment has been chosen to represent the results. In this scenario, the uncertainty in the distribution of the FE distribution arises from the combination of instrument calibration error and instrumental parameters.

show an increase trend. A significant selectivity switch can be observed for FE_{C2H4} and FE_{CH4} in each cycle. The exception is FE_{CO}, which is stabilized at around 10 % after the first restart (81 min). The sputtered Cu GDE shows comparable catalytic performance with respect to the best reported results in the literature (Table S2).

The performance restoration at each restart could be related to the recovery of the local environment during the current interruption. When the electrode is polarized, K^+ cations become enriched near the electrode due to the electrostatic force, and the higher local concentration of K^+ leads to salt deposition on the catalyst layer [56]. Salt deposition can block active sites and hinder mass diffusion, altering the local environment and consequently shifting the selectivity toward H_2 evolution. When polarization is interrupted, some of the salt can dissolve as the K^+ concentration decreases due to the loss of electrostatic forces. The recovery of the local environment could explain the restoration of CO_2RR selectivity after restarting. However, it does not fully explain the significant selectivity switch between C_2H_4 and CH_4. In addition, the CO selectivity is not recovered after the first restart. Hence, it is hypothesized that the interruption-restart process could also recover the material properties that influence the selectivity of CO_2RR. When the potential is removed, the catalyst surface likely gets oxidized due to the alkaline environment [49]. Several studies, especially applying a pulsed potential, confirm the instantaneous formation of oxide species on the surface [52,57]. The intermediate oxide species Cu_2O is very selective for C_{2+} products. The oxygen presence could be related to different species like Cu_2O, interstitial and vacancy oxygen [48]. Its presence could induce tensile strain and a defective rich surface with a high content of grain boundaries [58]. Also, different intermediate copper species are possible: CuO, $Cu(OH)_2$ and $Cu_2(OH)_2CO_3$ that favor the dimerization process. The dimerization process is based on the presence of a small presence of Cu^+ grains that favor the process. The catalyst transition to its reduced state Cu(0) reduces the active sites for dimerization, favoring the CH_4 production, and a further reduction extinguishes the selectivity towards CO_2RR products [58]. Additionally, the material properties responsible for the dimerization differ from those for the CO production [52]. The restart procedure cannot reconstruct the original oxide on the catalyst surface [29], thus probably strictly related to CO production losses. To explore this hypothesis Cu_{800} was prepared with the same procedure and stored in a glove box, and the exposure to atmosphere was less than 30 min before test. As shown in Fig. S7, the FE_{CO} on this sample is as low as 10 % at the beginning. Hence, it is likely that the interruption and restart process cannot recover all (sub)surface oxides that are related to the initially high CO production.

It has been postulated that the oxidation state of copper plays an important role in its electrocatalytic selectivity, with some showing correlations between Cu (I/II) oxides and increased selectivity for 76 % for C_{2+} products [29]. It has also been suggested that periodically altering the electrode potential (e.g. by pulsing) is a route towards stabilizing oxidized forms of copper and preventing its full reduction, thereby increasing selectivity towards C_{2+} products [57]. In this study, our strategy of periodically resting at open circuit exposes the Cu catalysts to an oxidizing combination of potential and local pH, so we hypothesized that electrode re-oxidation may be important to the trends in selectivity and stability we observed. To determine the catalyst oxidation state as a function of operation condition, we employed *operando* XAS at the Cu K-edge. Using a modified GDE flow cell with an X-ray transparent window added at the cathode flow field (see SI for details), we examined Cu_{800} electrodes under CO_2 reduction conditions at 200 mA cm^{-2}, both with and without application of the periodic rest periods. Under each condition, spectra were repeatedly acquired over time, and the trends are shown in Fig. 7 (additional data in Fig. S8). Under the initially dry condition, the spectrum suggests mixed oxide-metallic phases, due to natural oxidation of the Cu surface in air. When immersed in the electrolyte at open circuit before starting CO_2RR, the spectrum shows a significant increase in the Cu–O fraction, indicating rapid oxidation of the Cu electrode upon contact with the electrolyte. Upon starting CO_2RR, in every case the spectra gradually transform to resemble predominantly metallic Cu, a result of the strong reducing applied potentials. However, by looking at the Fourier-transformed extended X-ray absorption fine structure (FT-EXAFS, Fig. 7a) analysis, differences appear between the pulsed and non-pulsed experiments. In the latter case, the FT-EXAFS is dominated by a sharp peak at radial distance typical for Cu–Cu bonding in metal, whereas in the pulsed experiment this is accompanied by a small peak at shorter distance typical of Cu–O bonding in oxides. Linear combination fitting of the near-edge spectra with respect to standards of different Cu oxidation states further showed that periodically pausing the CO_2RR led to more persistent Cu (II) species, in correlation with more stable C_2H_4 selectivity and H_2 suppression (Fig. 7c). The differences in the performance (compared to above) could be attributable to the different cell geometry for this custom *operando* cell, but in general the results provide evidence of correlation between selectivity, stability, and the increased persistence of oxidized Cu. Since in this case XAS is a bulk-sensitive technique, the results cannot be used to precisely quantify the surface species and discern the exact catalytic active sites, but the general observation that Cu–O bonding persists when using the pulsing approach suggests that it may indeed be acting to re-generate and/or stabilize oxidized copper motifs at the electrocatalytic interface. It is reported in the literature that

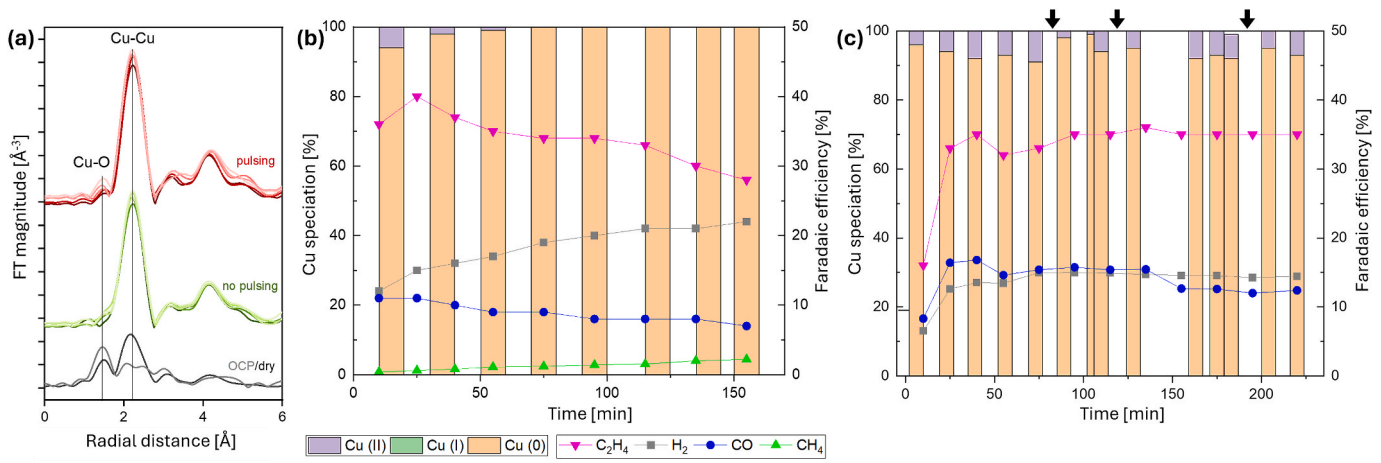

Fig. 7. *Operando* X-ray absorption spectroscopy (Cu k-edge) on Cu_{800} GDEs during CO_2RR at 200 mA cm^{-2}. (a) FT-EXAFS spectra from repeated measurements under pulsing (red) or constant (green) operation, with comparison to the pre-experiment spectra when dry and at OCP in the cell. Spectra were repeatedly acquired at an interval of about 17 min (reflected by the colour gradients from dark to light). Characteristic distances for Cu–O (in oxides) and Cu–Cu (in Cu metal) are indicated with vertical lines. Copper speciation (stacked bars, from fitting of XANES data) and measured Faradaic efficiency (symbols) for cells under (b) continuous operation, and (c) operation with intermittent pausing at open circuit (times indicated with black arrows).

the synergism of Cu metal/oxidized Cu pairs enhance the CO_2RR activity. Cu metal activates CO_2 and facilitates the following electron transfers, while the oxidized Cu strengthens *CO adsorption to further boost C–C coupling [59–61]. The density functional theory modelling [62,63] and recent experimental infrared spectroscopy and in situ XAS data [64] also suggested that the asymmetry between CO adsorption energies on metallic and oxidized copper sites facilitates CO dimerization and is essential for C_2 product formation. Based on our experimental observations and supporting literature, it is reasonable to conclude that the stable C_2H_4 products are correlated with the persistence of Cu cations under pulsing operation.

3.4. *Effects of electrolyte composition on CO_2RR performance*

Further investigations have been conducted to explore the effects of pH and K^+ concentrations on catalyst performance of Cu_{800}. A solution of 0.5 M KOH+0.025 M K_2SO_4 was studied to compare with 0.5 M KOH one. In this case, the pH value is similar for the two solutions, but the concentration of K^+ varies. In 0.5 M KOH (Fig. 8a), the electrode maintains a constant selectivity of 36 % towards C_2H_4 and is stable for over 150 min. When the electrolyte composition is 0.5 M KOH+0.025 M K_2SO_4 (Fig. 8b), the selectivity towards FE_{C2H4} reaches 42 % and is also stable for 150 min. The selectivity for other products remains stable in

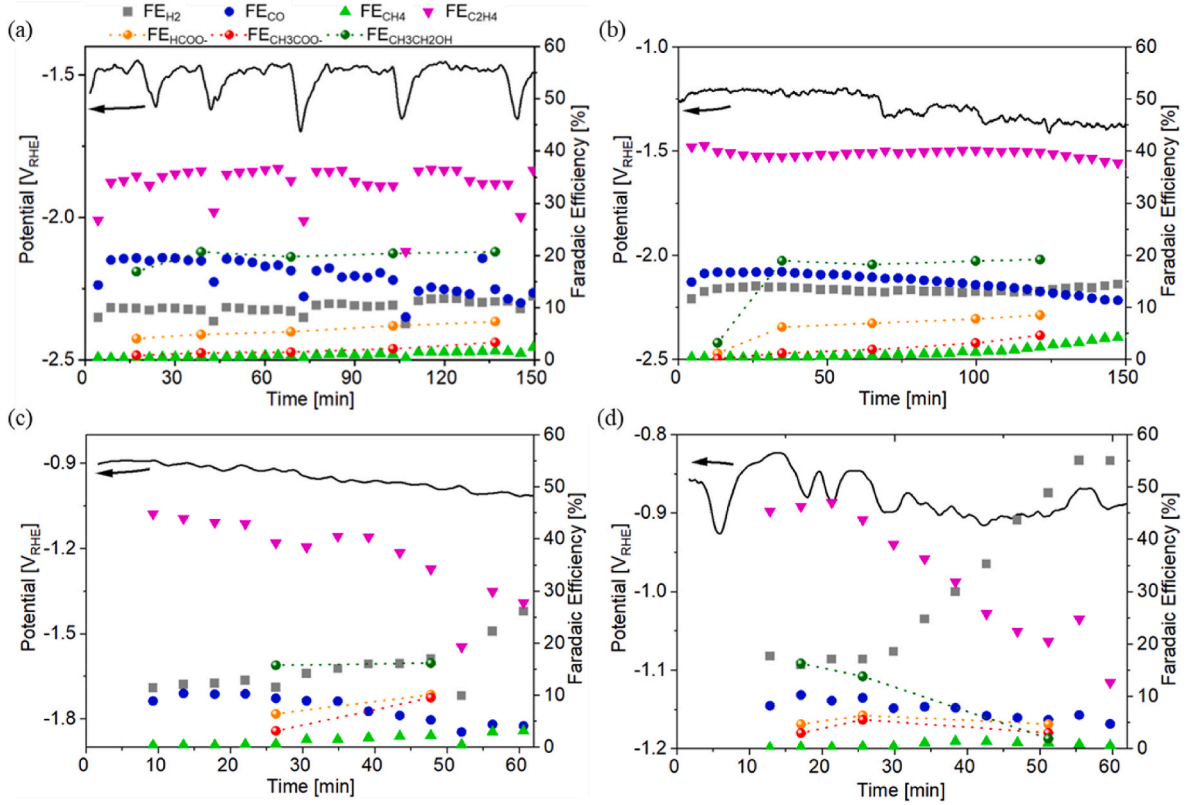

Fig. 8. CO_2RR on Cu_{800} a 200 mA cm^{-2} tested in various electrolytes: (a) 0.5 M KOH, (b) 0.5 M KOH + 0.25 M K_2SO_4, (c) 2 M KOH, (d) 3 M KOH.

both electrolytes. This outcome suggests that a higher K^+ concentration can slightly enhance the C_2H_4 selectivity, but it has no benefits on the stability. In 0.5 M KOH+0.025 M K_2SO_4 electrolyte, the selectivity is perfectly in line with those obtained in 1 M KOH (Fig. 5a). However, the former condition shows a significant enhancement in the stability. Hence, the pH seems to be a key factor that influences the stability. To better illustrate this correlation, the Cu electrode was further test in 1 M $KHCO_3$ electrolyte. As shown in Fig. S9, the stability for C_2H_4 formation is significantly enhanced to more than 300 min. These results highlight that the stability is critically dependent on the pH, but less related to the concentration of K^+ in the electrolyte in the investigated pH and [K^+] ranges. Instead, a higher K^+ can increase the C_2H_4 selectivity, reinforcing the active role of K^+ in the dimerization process.

With increasing the KOH molarity to 2 M, the initial selectivity increases up to 44 % (Fig. 8c), which is further enhanced to 47 % in 3 M KOH (Fig. 8d). The small enhancement in FE_{C2H4} could be due to the higher K^+ concentration [65], but probably also to the significantly lower H^+ availability [2,66]. In both 2 M and 3 M KOH, the stability is rapidly lost. It is further suggested that the stability is mainly ruled by the electrolyte pH, in agreement with the literature [67]. A possible explanation of the reduction of stability at higher pH could be attributed to the faster loss of Cu oxide species due to the instability of the catalyst at these conditions, as evidenced in the Pourbaix diagram [68]. This could be a further evidence of the key role of the oxide species effect on the dimerization process. The low stability at high bulk pH could also be related to the faster salt deposition due to the chemical interaction between CO_2 and OH^- at electrode/electrolyte interface. However, this is not considered severe, as we did not observe significant CO_2 loss using a mass flow meter measuring the gas flow at the outlet of the cathodic side during the test, nor visible salt precipitation on the post-mortem samples. Hence, the rapid failure of the electrodes at very high pH is likely due to the instability of the materials.

4. Conclusion

In this work, we reported simply prepared Cu-based GDEs for C_2H_4 production by electrochemically reducing CO_2. Different factors, including catalyst thickness, test protocol, and electrolyte can significantly affect the performance of the GDEs. A thicker Cu layer leads to enhanced selectivity toward C_2H_4 and CH_3CH_2OH products. On the optimal GDE, a maximum FE_{C2H4} up to 46 % and a C_2H_4 partial current of 216 mA cm^{-2} are achieved. The FE_{C2} is enhanced to a maximum of 70 % with a partial current density of 433 mA cm^{-2}. Despite these promising behaviors, the Cu GDEs degrade fast during the test, observing firstly a selectivity switch where FE_{C2H4} and $FE_{CH3CH2OH}$ decreases while FE_{CH4} and FE_{H2} increases, followed by electrode failure. A test protocol with current interruption followed by a restart can effectively recover the C_2H_4 and CH_3CH_2OH selectivity and prolong the operation time. *Operando* X-ray absorption spectroscopy study reveals that this protocol can retain a small fraction of oxidized Cu species in the Cu GDEs for a long time, which is probably responsible for the more stable production of C_2 products. The effects of cation concentration and pH of the electrolyte were also studied. The K^+ concentration slightly influences the C_2H_4 selectivity, but it does not seem to affect the stability in the investigated range. In contrast, the pH shows drastic effect on the stability, particularly at high pH values, likely due to the instability of Cu GDE in such alkaline solutions. This work provides comprehensive insights into the stability challenges of Cu GDEs for CO_2RR, offering guidance for future efforts to enhance the lifespan of Cu GDEs for C_2 production.

CRediT authorship contribution statement

Nicolò B.D. Monti: Writing – review & editing, Writing – original draft, Visualization, Validation, Methodology, Investigation, Formal analysis, Data curation, Conceptualization. **Gumaa A. El-Nagar:** Writing – review & editing, Validation, Investigation. **Marco Fontana:** Writing – review & editing, Investigation, Formal analysis. **Felicia Di Costola:** Writing – review & editing, Writing – original draft, Investigation, Data curation. **Siddharth Gupta:** Writing – review & editing, Investigation. **Matthew T. Mayer:** Writing – review & editing, Writing – original draft, Validation, Supervision, Resources, Methodology, Funding acquisition. **Candido F. Pirri:** Writing – review & editing, Supervision, Resources, Funding acquisition. **Juqin Zeng:** Writing – review & editing, Writing – original draft, Visualization, Validation, Supervision, Methodology, Investigation, Data curation, Conceptualization.

Supporting information

Supporting Information is available from the Wiley Online Library or from the author. The supporting information (SI) includes a schematic of the set-up for CO_2 electrolysis, schematic and photo of catholyte-flow cell adapted for *operando* XAS, geometric current density on Cu electrodes with different thickness tested in 1 M KOH at −1.2 V_{RHE}, electrochemical double layer capacitance (EDL) of Cu GDEs Samples obtained in a flow cell with 1 M KOH, selectivity as a function of time on various electrodes for different products during the CO_2RR test at −1.2 V_{RHE} with 1 M KOH electrolyte, faradaic efficiency on Cu GDE sample stored in Ar atmosphere, gaseous faradaic efficiencies as a function of time and chronoamperometry for Cu800 cathodes collected under pulsing and no pulsing conditions during XAS measurements and Product distribution as function of time on Cu_{800} at 200 mA cm^{-2} in 1 M $KHCO_3$.

Declaration of competing interest

The authors declare the following financial interests/personal relationships which may be considered as potential competing interests: Juqin Zeng reports financial support was provided by Italian Ministry of University and Research. Matthew T. Mayer reports financial support was provided by Helmholtz Association Initiative and Networking Fund. Matthew T. Mayer reports financial support was provided by European Union. If there are other authors, they declare that they have no known competing financial interests or personal relationships that could have appeared to influence the work reported in this paper.

Acknowledgements

Juqin Zeng received fund under the National Recovery and Resilience Plan (NRRP), Mission 4 “Education and Research” - Component 2 “From research to business” - Investment 3.1 “Fund for the realization of an integrated system of research and innovation infrastructures” - Call n. 3264 of December 28, 2021 of Italian Ministry of University and Research | Award Decree n. 128 (June 21, 2022)- Project code: IR0000027, Concession Decree No. 128 of June 21, 2022 adopted by the Italian Ministry of Research, CUP: B33C22000710006, Project title: iENTRANCE. This work was also supported by the Helmholtz Association Initiative and Networking Fund (Helmholtz Young Investigator Group VH-NH-1225), and by the European Union’s Horizon 2020 research and innovation program project FlowPhotoChem (grant agreement 862453). The material presented and views expressed here are the responsibilities of the author(s) only; the EU Commission takes no responsibility for any use made of the information set out. We thank the Helmholtz-Zentrum Berlin für Materialien und Energie for the allocation of synchrotron radiation beamtime at BESSY II.

Appendix A. Supplementary data

Supplementary data to this article can be found online at https://doi.org/10.1016/j.mtsust.2025.101124.

Data availability

Data will be made available on request.

References

[1] T. Ahmad, S. Liu, M. Sajid, K. Li, M. Ali, L. Liu, W. Chen, Electrochemical CO2 reduction to C2+ products using Cu-based electrocatalysts: a review, Nano Res. Energy 1 (2022), https://doi.org/10.26599/NRE.2022.9120021.

[2] Y. Zheng, A. Vasileff, X. Zhou, Y. Jiao, M. Jaroniec, S.Z. Qiao, Understanding the roadmap for electrochemical reduction of CO2 to multi-carbon oxygenates and hydrocarbons on copper-based catalysts, J. Am. Chem. Soc. 141 (2019) 7646–7659, https://doi.org/10.1021/jacs.9b02124.

[3] N.B.D. Monti, M. Fontana, A. Sacco, A. Chiodoni, A. Lamberti, C.F. Pirri, J. Zeng, Facile fabrication of Ag electrodes for CO2-to-CO conversion with near-unity selectivity and high mass activity, ACS Appl. Energy Mater. 5 (2022) 14779–14788, https://doi.org/10.1021/acsaem.2c02143.

[4] M.A.O. Lourenco, J. Zeng, P. Jagdale, M. Castellino, A. Sacco, M.A. Farkhondehfal, C.F. Pirri, Biochar/zinc oxide composites as effective catalysts for electrochemical CO2Reduction, ACS Sustain. Chem. Eng. 9 (2021) 5445–5453, https://doi.org/10.1021/acssuschemeng.1c00837.

[5] A. Sacco, R. Speranza, U. Savino, J. Zeng, M.A. Farkhondehfal, A. Lamberti, A. Chiodoni, C.F. Pirri, An integrated device for the solar-driven electrochemical conversion of CO2to CO, ACS Sustain. Chem. Eng. 8 (2020) 7563–7568, https://doi.org/10.1021/acssuschemeng.0c02088.

[6] J. Zeng, M.R. Fiorentin, M. Fontana, M. Castellino, F. Risplendi, A. Sacco, G. Cicero, M.A. Farkhondehfal, F. Drago, C.F. Pirri, Novel insights into Sb-Cu catalysts for electrochemical reduction of CO2, Appl. Catal., B 306 (2022), https://doi.org/10.1016/j.apcatb.2022.121089.

[7] J. Zeng, P. Jagdale, M.A.O. Lourenço, M. Amin Farkhondehfal, D. Sassone, M. Bartoli, C. Fabrizio Pirri, Biochar-Supported BiO X for Effective Electrosynthesis of Formic Acid from Carbon Dioxide Reduction, vol. 11, 2021, p. 363, https://doi.org/10.3390/cryst.

[8] K. Bejtka, N.B.D. Monti, A. Sacco, M. Castellino, S. Porro, M.A. Farkhondehfal, J. Zeng, C.F. Pirri, A. Chiodoni, Zn- and Ti-doped SnO2 for enhanced electroreduction of carbon dioxide, Materials 14 (2021), https://doi.org/10.3390/ma14092354.

[9] K. Bejtka, J. Zeng, A. Sacco, M. Castellino, S. Hernández, M.A. Farkhondehfal, U. Savino, S. Ansaloni, C.F. Pirri, A. Chiodoni, Chainlike mesoporous SnO2 as a well-performing catalyst for electrochemical CO2 reduction, ACS Appl. Energy Mater. 2 (2019) 3081–3091, https://doi.org/10.1021/acsaem.8b02048.

[10] J. Zeng, K. Bejtka, W. Ju, M. Castellino, A. Chiodoni, A. Sacco, M.A. Farkhondehfal, S. Hernández, D. Rentsch, C. Battaglia, C.F. Pirri, Advanced Cu-Sn foam for selectively converting CO2 to CO in aqueous solution, Appl. Catal., B 236 (2018) 475–482, https://doi.org/10.1016/j.apcatb.2018.05.056.

[11] N.B.D. Monti, J. Zeng, M. Castellino, S. Porro, M. Bagheri, C.F. Pirri, A. Chiodoni, K. Bejtka, Effects of annealing conditions on the catalytic performance of anodized tin oxide for electrochemical carbon dioxide reduction, Nanomaterials 15 (2025) 121, https://doi.org/10.3390/nano15020121.

[12] K. Fernández-Caso, G. Díaz-Sainz, M. Alvarez-Guerra, A. Irabien, Electroreduction of CO2: advances in the continuous production of formic acid and formate, ACS Energy Lett. 8 (2023) 1992–2024, https://doi.org/10.1021/acsenergylett.3c00489.

[13] J. Cai, Q. Zhao, W.Y. Hsu, C. Choi, Y. Liu, J.M.P. Martirez, C. Chen, J. Huang, E. A. Carter, Y. Huang, Highly selective electrochemical reduction of CO2 into methane on nanotwinned Cu, J. Am. Chem. Soc. 145 (2023) 9136–9143, https://doi.org/10.1021/jacs.3c00847.

[14] J. Zeng, M. Mignosa, N.B.D. Monti, A. Sacco, C.F. Pirri, Engineering copper nanoparticle electrodes for tunable electrochemical reduction of carbon dioxide, Electrochim. Acta 464 (2023), https://doi.org/10.1016/j.electacta.2023.142862.

[15] D. Ren, Y. Deng, A.D. Handoko, C.S. Chen, S. Malkhandi, B.S. Yeo, Selective electrochemical reduction of carbon dioxide to ethylene and ethanol on copper(I) oxide catalysts, ACS Catal. 5 (2015) 2814–2821, https://doi.org/10.1021/cs502128q.

[16] X. Chen, J. Chen, N.M. Alghoraibi, D.A. Henckel, R. Zhang, U.O. Nwabara, K. E. Madsen, P.J.A. Kenis, S.C. Zimmerman, A.A. Gewirth, Electrochemical CO2-to-ethylene conversion on polyamine-incorporated Cu electrodes, Nat. Catal. 4 (2021) 20–27, https://doi.org/10.1038/s41929-020-00547-0.

[17] J. Kim, W. Choi, J.W. Park, C. Kim, M. Kim, H. Song, Branched copper oxide nanoparticles induce highly selective ethylene production by electrochemical carbon dioxide reduction, J. Am. Chem. Soc. 141 (2019) 6986–6994, https://doi.org/10.1021/jacs.9b00911.

[18] Y. Ouyang, L. Shi, X. Bai, C. Ling, Q. Li, J. Wang, Selectivity of electrochemical CO2 reduction toward ethanol and ethylene: the key role of surface-active hydrogen, ACS Catal. 13 (2023) 15448–15456, https://doi.org/10.1021/acscatal.3c03797.

[19] Z. Tang, E. Nishiwaki, K.E. Fritz, T. Hanrath, J. Suntivich, Cu(I) reducibility controls ethylene vs ethanol selectivity on (100)-textured copper during pulsed CO2Reduction, ACS Appl. Mater. Interfaces 13 (2021) 14050–14055, https://doi.org/10.1021/acsami.0c17668.

[20] Y.C. Li, Z. Wang, T. Yuan, D.H. Nam, M. Luo, J. Wicks, B. Chen, J. Li, F. Li, F.P. G. De Arquer, Y. Wang, C.T. Dinh, O. Voznyy, D. Sinton, E.H. Sargent, Binding site diversity promotes CO2 electroreduction to ethanol, J. Am. Chem. Soc. 141 (2019) 8584–8591, https://doi.org/10.1021/jacs.9b02945.

[21] J. Sisler, S. Khan, A.H. Ip, M.W. Schreiber, S.A. Jaffer, E.R. Bobicki, C.T. Dinh, E. H. Sargent, Ethylene electrosynthesis: a comparative techno-economic analysis of alkaline vs membrane electrode assembly vs CO2-CO-C2H4Tandems, ACS Energy Lett. 6 (2021) 997–1002, https://doi.org/10.1021/acsenergylett.0c02633.

[22] Y. Hori, H. Wakebe, T. Tsukamoto, O. Koga, Electrocatalytic process of CO selectivity in electrochemical reduction of CO2 at metal electrodes in aqueous media, Electrochim. Acta 39 (1994) 1833–1839, https://doi.org/10.1016/0013-4686(94)85172-7.

[23] A.A. Peterson, F. Abild-Pedersen, F. Studt, J. Rossmeisl, J.K. Nørskov, How copper catalyzes the electroreduction of carbon dioxide into hydrocarbon fuels, Energy Environ. Sci. 3 (2010) 1311–1315, https://doi.org/10.1039/c0ee00071j.

[24] A.A. Peterson, J.K. Nørskov, Activity descriptors for CO 2 electroreduction to methane on transition-metal catalysts, J. Phys. Chem. Lett. 3 (2012) 251–258, https://doi.org/10.1021/jz201461p.

[25] C.-T. Dinh, T. Burdyny, M.G. Kibria, A. Seifitokaldani, C.M. Gabardo, F. Pelayo García De Arquer, A. Kiani, J.P. Edwards, P. De Luna, O.S. Bushuyev, C. Zou, R. Quintero-Bermudez, Y. Pang, D. Sinton, E.H. Sargent, CO 2 electroreduction to ethylene via hydroxide-mediated copper catalysis at an abrupt interface, n.d. https://www.science.org.

[26] W. Ma, S. Xie, T. Liu, Q. Fan, J. Ye, F. Sun, Z. Jiang, Q. Zhang, J. Cheng, Y. Wang, Electrocatalytic reduction of CO2 to ethylene and ethanol through hydrogen-assisted C–C coupling over fluorine-modified copper, Nat. Catal. 3 (2020) 478–487, https://doi.org/10.1038/s41929-020-0450-0.

[27] M. Zhong, K. Tran, Y. Min, C. Wang, Z. Wang, C.T. Dinh, P. De Luna, Z. Yu, A. S. Rasouli, P. Brodersen, S. Sun, O. Voznyy, C.S. Tan, M. Askerka, F. Che, M. Liu, A. Seifitokaldani, Y. Pang, S.C. Lo, A. Ip, Z. Ulissi, E.H. Sargent, Accelerated discovery of CO2 electrocatalysts using active machine learning, Nature 581 (2020) 178–183, https://doi.org/10.1038/s41586-020-2242-8.

[28] J. Zeng, M. Castellino, M. Fontana, A. Sacco, N.B.D. Monti, A. Chiodoni, C.F. Pirri, Electrochemical reduction of CO2 with good efficiency on a nanostructured Cu-Al catalyst, Front. Chem. 10 (2022), https://doi.org/10.3389/fchem.2022.931767.

[29] R.M. Arán-Ais, F. Scholten, S. Kunze, R. Rizo, B. Roldan Cuenya, The role of in situ generated morphological motifs and Cu(i) species in C2+ product selectivity during CO2 pulsed electroreduction, Nat. Energy 5 (2020) 317–325, https://doi.org/10.1038/s41560-020-0594-9.

[30] W. Tang, A.A. Peterson, A.S. Varela, Z.P. Jovanov, L. Bech, W.J. Durand, S. Dahl, J. K. Nørskov, I. Chorkendorff, The importance of surface morphology in controlling the selectivity of polycrystalline copper for CO2 electroreduction, Phys. Chem. Chem. Phys. 14 (2012) 76–81, https://doi.org/10.1039/C1CP22700A.

[31] A. Dutta, M. Rahaman, N.C. Luedi, M. Mohos, P. Broekmann, Morphology matters: tuning the product distribution of CO2 electroreduction on oxide-derived Cu foam catalysts, ACS Catal. 6 (2016) 3804–3814, https://doi.org/10.1021/acscatal.6b00770.

[32] Y. Yang, Y. Shi, H. Yu, J. Zeng, K. Li, F. Li, Mitigating carbonate formation in CO2 electrolysis, Next Energy 1 (2023) 100030, https://doi.org/10.1016/j.nxener.2023.100030.

[33] W. Lai, Y. Qiao, Y. Wang, H. Huang, Stability issues in electrochemical CO2 reduction: recent advances in fundamental understanding and design strategies, Adv. Mater. 35 (2023), https://doi.org/10.1002/adma.202306288.

[34] Q. Chang, J.H. Lee, Y. Liu, Z. Xie, S. Hwang, N.S. Marinkovic, A.H.A. Park, S. Kattel, J.G. Chen, Electrochemical CO2Reduction reaction over Cu nanoparticles with tunable activity and selectivity mediated by functional groups in polymeric binder, JACS Au 2 (2022) 214–222, https://doi.org/10.1021/jacsau.1c00487.

[35] F. Jiao, J. Biener, E. Jeng, Z. Qi, A.R. Kashi, S. Hunegnaw, Z. Huo, J.S. Miller, L. B. Bayu Aji, B.H. Ko, H. Shin, S. Ma, K.P. Kuhl, Scalable gas diffusion electrode fabrication for electrochemical CO2 reduction using physical vapor deposition methods, ACS Appl. Mater. Interfaces 14 (2022) 7731–7740, https://doi.org/10.1021/acsami.1c17860.

[36] A.R.T. Morrison, N. Girichandran, Q. Wols, R. Kortlever, Design of an elevated pressure electrochemical flow cell for CO2 reduction, J. Appl. Electrochem. 53 (2023) 2321–2330, https://doi.org/10.1007/s10800-023-01927-7.

[37] C.M. Gabardo, C.P. O'Brien, J.P. Edwards, C. McCallum, Y. Xu, C.T. Dinh, J. Li, E. H. Sargent, D. Sinton, Continuous carbon dioxide electroreduction to concentrated multi-carbon products using a membrane electrode assembly, Joule 3 (2019) 2777–2791, https://doi.org/10.1016/j.joule.2019.07.021.

[38] J. Zeng, J.R. Nair, C. Francia, S. Bodoardo, N. Penazzi, Aprotic Li-O2 cells: gas diffusion layer (GDL) as catalyst free cathode and tetraglyme/LiClO4 as electrolyte, Solid State Ionics 262 (2014) 160–164, https://doi.org/10.1016/j.ssi.2013.09.032.

[39] S. Vankova, C. Francia, J. Amici, J. Zeng, S. Bodoardo, N. Penazzi, G. Collins, H. Geaney, C. O'Dwyer, Influence of binders and solvents on stability of Ru/RuOx nanoparticles on ITO nanocrystals as Li–O2 battery cathodes, ChemSusChem 10 (2017) 575–586, https://doi.org/10.1002/cssc.201601301.

[40] S. Martinez Crespiera, D. Amantia, E. Knipping, C. Aucher, L. Aubouy, J. Amici, J. Zeng, C. Francia, S. Bodoardo, Electrospun Pd-doped mesoporous carbon nano fibres as catalysts for rechargeable Li-O2 batteries, RSC Adv. 6 (2016) 57335–57345, https://doi.org/10.1039/c6ra09721a.

[41] D.M. Többens, S. Zander, KMC-2: an X-ray beamline with dedicated diffraction and XAS endstations at BESSY II, J. Large-Scale Res. Facil. JLSRF 2 (2016) A49, https://doi.org/10.17815/jlsrf-2-65.

[42] G.A. El-Nagar, F. Haun, S. Gupta, S. Stojkovikj, M.T. Mayer, Unintended cation crossover influences CO2 reduction selectivity in Cu-based zero-gap electrolysers, Nat. Commun. 14 (2023), https://doi.org/10.1038/s41467-023-37520-x.

[43] A. Dutta, M. Rahaman, M. Mohos, A. Zanetti, P. Broekmann, Electrochemical CO2 conversion using skeleton (sponge) type of Cu catalysts, ACS Catal. 7 (2017) 5431–5437, https://doi.org/10.1021/acscatal.7b01548.

[44] C.S. Chen, A.D. Handoko, J.H. Wan, L. Ma, D. Ren, B.S. Yeo, Stable and selective electrochemical reduction of carbon dioxide to ethylene on copper mesocrystals, Catal. Sci. Technol. 5 (2015) 161–168, https://doi.org/10.1039/c4cy00906a.
[45] G.L. De Gregorio, T. Burdyny, A. Loiudice, P. Iyengar, W.A. Smith, R. Buonsanti, Facet-dependent selectivity of Cu catalysts in electrochemical CO2 reduction at commercially viable current densities, ACS Catal. 10 (2020) 4854–4862, https://doi.org/10.1021/acscatal.0c00297.
[46] P. Mukherjee, K. Sathiyan, R.S. Vishwanath, T. Zidki, Anchoring MoS_2 on an ethanol-etched Prussian blue analog for enhanced electrocatalytic efficiency for the oxygen evolution reaction, Mater. Chem. Front. 6 (2022) 1770–1778, https://doi.org/10.1039/D2QM00183G.
[47] C.C.L. McCrory, S. Jung, J.C. Peters, T.F. Jaramillo, Benchmarking heterogeneous electrocatalysts for the oxygen evolution reaction, J. Am. Chem. Soc. 135 (2013) 16977–16987, https://doi.org/10.1021/ja407115p.
[48] H.Y. Wang, M. Soldemo, D. Degerman, P. Lömker, C. Schlueter, A. Nilsson, P. Amann, Direct evidence of subsurface oxygen formation in oxide-derived Cu by X-ray photoelectron spectroscopy, Angew. Chem. Int. Ed. 61 (2022), https://doi.org/10.1002/anie.202111021.
[49] F. Cavalca, R. Ferragut, S. Aghion, A. Eilert, O. Diaz-Morales, C. Liu, A.L. Koh, T. W. Hansen, L.G.M. Pettersson, A. Nilsson, Nature and distribution of stable subsurface oxygen in copper electrodes during electrochemical CO2 reduction, J. Phys. Chem. C 121 (2017), https://doi.org/10.1021/acs.jpcc.7b08278.
[50] C.W. Li, J. Ciston, M.W. Kanan, Electroreduction of carbon monoxide to liquid fuel on oxide-derived nanocrystalline copper, Nature 508 (2014) 504–507, https://doi.org/10.1038/nature13249.
[51] M. Li, M.N. Idros, Y. Wu, T. Burdyny, S. Garg, X.S. Zhao, G. Wang, T.E. Rufford, The role of electrode wettability in electrochemical reduction of carbon dioxide, J Mater Chem A Mater 9 (2021) 19369–19409, https://doi.org/10.1039/d1ta03636j.
[52] H.S. Jeon, J. Timoshenko, C. Rettenmaier, A. Herzog, A. Yoon, S.W. Chee, S. Oener, U. Hejral, F.T. Haase, B. Roldan Cuenya, Selectivity control of Cu nanocrystals in a gas-fed flow cell through CO2Pulsed electroreduction, J. Am. Chem. Soc. 143 (2021) 7578–7587, https://doi.org/10.1021/jacs.1c03443.
[53] B. Schmid, C. Reller, S. Neubauer, M. Fleischer, R. Dorta, G. Schmid, Reactivity of copper electrodes towards functional groups and small molecules in the context of CO2 electro-reductions, Catalysts 7 (2017) 161, https://doi.org/10.3390/catal7050161.
[54] A. Engelbrecht, C. Uhlig, O. Stark, M. Hämmerle, G. Schmid, E. Magori, K. Wiesner-Fleischer, M. Fleischer, R. Moos, On the electrochemical CO 2 reduction at copper sheet electrodes with enhanced long-term stability by pulsed electrolysis, J. Electrochem. Soc. 165 (2018) J3059–J3068, https://doi.org/10.1149/2.0091815jes.
[55] J. Kok, J. de Ruiter, W. van der Stam, T. Burdyny, Interrogation of oxidative pulsed methods for the stabilization of copper electrodes for CO_2 electrolysis, J. Am. Chem. Soc. 146 (2024) 19509–19520, https://doi.org/10.1021/jacs.4c06284.
[56] A.B. Moss, S. Garg, M. Mirolo, C.A. Giron Rodriguez, R. Ilvonen, I. Chorkendorff, J. Drnec, B. Seger, In operando investigations of oscillatory water and carbonate effects in MEA-based CO2 electrolysis devices, Joule 7 (2023) 350–365, https://doi.org/10.1016/j.joule.2023.01.013.
[57] J. Timoshenko, A. Bergmann, C. Rettenmaier, A. Herzog, R.M. Arán-Ais, H.S. Jeon, F.T. Haase, U. Hejral, P. Grosse, S. Kühl, E.M. Davis, J. Tian, O. Magnussen, B. Roldan Cuenya, Steering the structure and selectivity of CO2 electroreduction catalysts by potential pulses, Nat. Catal. 5 (2022) 259–267, https://doi.org/10.1038/s41929-022-00760-z.
[58] Q. Lei, L. Huang, J. Yin, B. Davaasuren, Y. Yuan, X. Dong, Z.P. Wu, X. Wang, K. X. Yao, X. Lu, Y. Han, Structural evolution and strain generation of derived-Cu catalysts during CO2 electroreduction, Nat. Commun. 13 (2022), https://doi.org/10.1038/s41467-022-32601-9.
[59] X. Yuan, S. Chen, D. Cheng, L. Li, W. Zhu, D. Zhong, Zh Zhao, J. Li, T. Wang, J. Gong, Controllable Cu^0-Cu^+ sites for electrocatalytic reduction of carbon dioxide, Angew. Chem. Int. Ed. 60 (2021) 15344–15347, https://doi.org/10.1002/anie.202105118.
[60] X. Lv, Q. Liu, J. Wang, X. Wu, X. Li, Y. Yang, J. Yan, A. Wu, H. Wu, Grain refining enables mixed Cu+/Cu0 states for CO2 electroreduction to C2+ products at high current density, Appl. Catal. B Environ. 324 (2023) 122272, https://doi.org/10.1016/j.apcatb.2022.122272.
[61] K. Yue, Y. Qin, H. o Huang, Z. Lv, M. Cai, Y. Su, F. Huang, Y. Yan, Stabilized Cu0 -Cu1+ dual sites in a cyanamide framework for selective CO2 electroreduction to ethylene, Nat. Commun. 15 (2024) 7820, https://doi.org/10.1038/s41467-024-52022-0.
[62] S. Lin, C. Chang, S. Chiu, H. Pai, T. Liao, C. Hsu, W. Chiang, M. Tsai, H. Chen, Operando time-resolved X-ray absorption spectroscopy reveals the chemical nature enabling highly selective CO2 reduction, Nat. Commun. 11 (2020) 3525, https://doi.org/10.1038/s41467-020-17231-3.
[63] F. Dattila, R. García-Muelas, N. López, Active and selective ensembles in oxide-derived copper catalysts for CO2 reduction, ACS Energy Lett. 5 (2020) 3176–3184, https://doi.org/10.1021/acsenergylett.0c01777.
[64] T. Chou, C. Chang, H. Yu, W. Yu, C. Dong, J. Velasco-Vélez, C. Chuang, L. Chen, J. Lee, J. Chen, H. Wu, Controlling the oxidation state of the Cu electrode and reaction intermediates for electrochemical CO2 reduction to ethylene, J. Am. Chem. Soc. 142 (2020) 2857–2867, https://doi.org/10.1021/jacs.9b11126.
[65] J. Li, D. Wu, A.S. Malkani, X. Chang, M.J. Cheng, B. Xu, Q. Lu, Hydroxide is not a promoter of C2+ product formation in the electrochemical reduction of CO on copper, Angew. Chem. Int. Ed. 59 (2020) 4464–4469, https://doi.org/10.1002/anie.201912412.
[66] S.J. Shin, H. Choi, S. Ringe, D.H. Won, H.S. Oh, D.H. Kim, T. Lee, D.H. Nam, H. Kim, C.H. Choi, A unifying mechanism for cation effect modulating C1 and C2 productions from CO2 electroreduction, Nat. Commun. 13 (2022), https://doi.org/10.1038/s41467-022-33199-8.
[67] D.A. Henckel, M.J. Counihan, H.E. Holmes, X. Chen, U.O. Nwabara, S. Verma, J. Rodríguez-López, P.J.A. Kenis, A.A. Gewirth, Potential dependence of the local pH in a CO2 reduction electrolyzer, ACS Catal. 11 (2021) 255–263, https://doi.org/10.1021/acscatal.0c04297.
[68] S. Jiang, L. D'Amario, H. Dau, Copper carbonate hydroxide as precursor of interfacial CO in CO2 electroreduction, ChemSusChem 15 (2022), https://doi.org/10.1002/cssc.202102506.